STM JOURNALS

Journal of
Polymer & Composites

ISSN: 2321-2810 (Online)
ISSN: 2321-8525 (Print)
Volume 13, Special Issue 1, 2025
DOI (Journal): 10.37591/JoPC

https://journals.stmjournals.com/jopc

Research JoPC

Electrical Measurements on La-Modified Four-Layered Aurivillius Ceramics

Jyothirmai C[1], N.V. Prasad [2,*]

Abstract

Bismuth layered structure ferroelectric (BLSF) of Aurivillius family is found to be attractive owing to its scientific and technological point of view. These materials have potential ferroelectric applications owing to the fact of its high Curie temperature, high temperature piezo-devise and ferroelectric random access memory (FRAM), applications. In addition, Bi-modified compounds have shown improved ferroelectric properties. However, the plausible reason for improving ferroelectric properties in Bi-modified is still unclear. The present manuscript explains the structural and electric properties of La-modified strontium bismuth zirconium titanate (SBTZO; $SrLa_xBi_{4-x}Ti_{3.85}Zr_{0.15}O_{15}$, where x=0.15, 0.25, 0.50), prepared by solid-state reaction method. X-ray diffraction reveals the single-phase orthorhombic structure. SEM photographs revealed that the ceramics were composed with randomly oriented plate-like grains. The average grain size is found to increase with increasing La- composition. The Raman vibrational modes show the distribution of La into pseudo perovskite layers and Bi^{+3}, Sr^{+2} ions into Bi_2O_3 layers. Asymmetric impedance spectroscopic plots suggest the non-Debye relaxation. The charge carriers are found to be controlled thermally activated process. Depressed semicircles have shown both grain and grain boundary contributions Ac-conductivity data was found to fit in to the universal (Jonscher's) law. A decrease in the dielectric constant with increasing La-concentration is explained by means of oxygen vacancy concentration. The structural relaxation was attributed to the occupation of La into $(Bi_2O_3)^{+2}$ layers and the same is corroborated to the Raman spectroscopic data. The temperature dependent of dielectric study gives information about transition temperature. The broad dielectric peak suggests that the transition belongs to diffuse phase transition (DPT).

Keywords: Solid – state reaction method, XRD, Raman, impedance, AC conductivity

INTRODUCTION

Aurivillius layered perovskite of strontium bismuth titanate ($SrBi_4Ti_4O15$ SBT) found to be the most versatile in the development of actuators and sensors due to its orthorhombic structure, curie temperature, (>400^0C), high dielectric constant, high dielectric breakdown, low dielectric loss and high anisotropy nature [1]. The structural formula of the present Aurivillius layered perovskite is $(Bi_2O_2)^{2+}(A_{m-1}B_mO_{3m+1})^{2-}$,where the term A-represents divalent or trivalent cations, having coordination number 12. The term B- represents small size cation located in the octahedral of pseudo perovskite block and the layer number is represented by "m" in the above representation. The bismuth evaporation led to the creation of vacancies and may not maintain the charge neutrality condition. Therefore, the oxygen vacancies are the prime responsible for high conductivity in these layered-perovskites. In order to control the oxygen vacancy, many researchers are tailoring the ferroelectric properties by substituting different rare earth ions at A-site and tetravalent at B-site [2–5]. Among all the layered perovskites, SBT was found to be more suitable

***Author for Correspondence**
N.V. Prasad

[1]Research Scholar, Department of Physics, Osmania University, Hyderabad, Telangana, India
[2]Associate Professor, Department of Physics, Osmania University, Hyderabad, Telangana, India

Received Date: April 19, 2024
Accepted Date: May 09, 2024
Published Date: November 04, 2024

Citation: Jyothirmai C, N.V. Prasad. Electrical Measurements on La-modified Four-Layered Aurivillius Ceramics. Journal of Polymer & Composites. 2025; 13(Special Issue 1): S157–S170p.

material for stress-sensor devices working at high temperatures [6–10]. It is also reported that ferroelectric nature is mainly depends on the hybridization of B- site ion and oxygen site by means of B-O interaction. It is reported that the low concentration of Zr_x (x> 0.15) modified SBT has shown enhanced ferroelectric properties [10]. Moreover, B-site modification certainly improves the ferroelectric properties, Zr- modified $BaTiO_3$ and $PbTiO_3$ ceramics have shown enhanced electrical properties. It is a well-known fact that the partial modified A- site (Bi) with La ($SrBi_{4-x}La_xTi_4O_{15}$, x> 1) has shown enhanced electrical properties in BLSF materials. Keeping in view of this, we have prepared La and Zr-modified SBT, namely, $SrR_xBi_{4-x}Ti_{3.85}Zr_{0.15}O_{15}$ (where R_x=La and x=0.15, 0.25, 0.50). A detailed microstructure, electrical and impedance study is undertaken. This work motivates us to investigate the overall contribution of grain and grain boundaries to electrical properties.

EXPERIMENTAL STUDIES

$SrR_xBi_{4-x}Ti_{3.85}Zr_{0.15}O_{15}$ (where R_x=La and x=0.15, 0.25, 0.50) ceramics were prepared by using the conventional solid-state reaction method. In this method, we used high purity oxides of $SrCO_3$, Bi_2O_3, TiO_2, La_2O_3, ZrO_2 as the starting materials. The stoichiometric amount of oxides was mixed thoroughly. The mixtures were thoroughly grinded, in the presence of acetone medium, in a planetary ball mill for 12 hours. In addition, 2% of excess Bi_2O_3 was also added to the composition to compensate the bismuth evaporation, during the sintering process. After milling, the mixture was calcined at 900^{o}c for 4hr. The calcined powder was ground and then mixed with a binder (3% PVA). The powder was then pressed into circular discs of 10 mm diameter and 1mm thickness, using hydraulic pressure. Finally, the pellets were sintered at 1000^{o}c for 4hrs in a conventional furnace.

Phase analysis of samples was made by X-ray diffraction (XRD), using analytical X-ray diffractometer. The X-ray data was compared to the standard compound ICSD#51863.

Lattice parameters of compounds were calculated, based on the parent compound SBT. Surface morphology was analyzed using a scanning electron microscope SEM model-CARLZEISS-EVO18SEM. Impedance studies were measured with help of the Auto-Lab PGSTAT30 and NOVA11.1. Dielectric data and complex impedance data was extracted from the impedance data with the help of the following equations:

$$Z' = Z\cos\theta\ ,\ Z'' = -z\sin\theta \quad (1)$$

$$M^*=1/\varepsilon^*=j\omega c_o z^*;\ M'=j\omega c_o Z''\ \text{ and } M''=j\omega c_o Z' \quad (2)$$

$$\tan\delta = \varepsilon''/\varepsilon' \quad (3)$$

RESULTS AND DISCUSSIONS

X-ray Diffraction Studies

Figure 1 shows the X-ray powder Diffraction pattern of SLBTZO-0.15, SLBTZO-0.25 and SLBTZO-0.50 ceramics respectively. Preliminary analysis of XRD patterns reveals that all samples were formed in a single phase and all XRD reflections have been matched with parent and the standard XRD pattern, as shown in the Figure 1. The lattice parameters of all the samples calculated based on the SBT, were tabulated in Table 1.

Table 1. Lattice parameters, Orthorhombicity and volume of all samples.

	Lattice parameters			**Orthorhombicity**	**volume**
	a(Å)	b(Å)	c(Å)	2(a-b)/(a+b)	$V(Å)^3$
SLBTZO-0.15	5.44	5.42	40.98	0.0023	1207.72
SLBTZO-0.25	5.43	5.42	40.98	0.0022	1207.84
SLBTZO-0.50	5.43	5.41	40.98	0.0023	1206.28

The highest peak of all compounds is observed at (1 1 9) orientation, at nearly diffraction angle 30^0 of 2-theta. XRD patterns of all various La doped compositions show a single orthorhombic phase with C^{2v}_{12} ($A2_1am$) space group without any impurities or unwanted peaks. This demonstrates that lanthanum substitution does not affect the $(Bi_2O_2)^{2+}$ structure [9]. Lattice parameters were found to decrease with increasing La- content. For higher La- content, a slight decrease in lattice parameters is attributed to occupancy of the La^{3+} in $(Bi_2O_2)^{2+}$ layers. From the XRD peaks, it is observed that with the increase of La-doping concentration, the maximum intensity peak (1 1 9) and even peaks (2 0 0) and (0 0 16) where found to shift towards lower 2θ value. This could be attributed to the larger ionic radius of Zr- ion (0.72 Å) when compared to Ti -ion (0.06 Å). In addition, the degree of orientation (∝) is found to increase with increasing La^{3+} concentration. The degree of orientation (∝) can be calculated by using the following relation.

$$\propto = \frac{I(200)}{I(200)+I(119)} \quad (4)$$

Where I (119) and I(200) represents the intensities of (119) and (200) XRD peaks. It is reported that the Bi^{3+} ion and O^{2-} ion vacancies were found to decrease with La^{3+} doping. The same can be corroborated to the tolerance factor and decreasing average ion ratio of Bi and La ions. From this, one can speculate that with the increasing trend of ∝ changes the spectrum from orthorhombic to tetragonal. Lattice parameters and cell volume were found to decrease with the increasing of the La- content. This clearly indicates the lattice distortion of the pseudo-perovskite layer compounds. The above results are diametrically different, compared to the earlier results when Zr substituted SBT.

Morphological Analysis

The scanning electron microscope image gives the information about surface morphology of ceramics. The microstructure shows well-bounded grains with less porosity. SEM structure Figure 2(a-c) shows the combination of both needle and plate like grains, around 1µm. All grains were found to be different sizes. Inset Figure 2(a-c) shows a histogram of grain sizes and the data is well fitted with the Gaussian curve. The mean size of the grains was found to be – 1.07µm for SLBTZO-0.15, 0.82 µm for SLBTZO-0.25, 1.03 µm for SLBTZO-0.50 respectively. The length and breadth of all grains were found to be large in size, compared to the thickness. This is a clear indication of preferred grain growth along c-axis. The plate-like morphology is attributed to the lower surface energy of (0 0 *l*) plane and finally results into plate-like growth morphology only a-b direction [10].

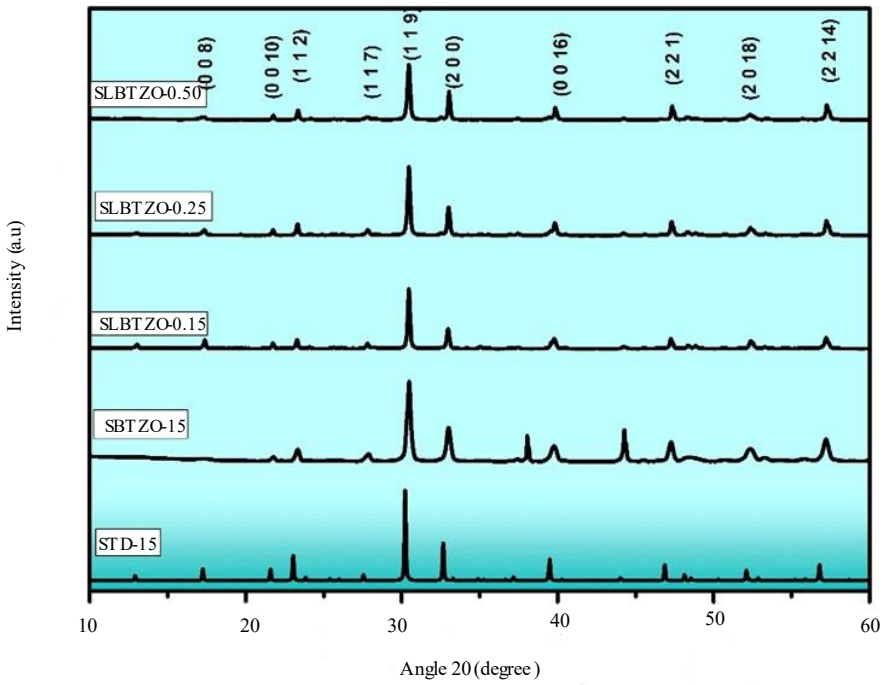

Figure1. The XRD pattern of SLBTZO-0.15, SLBTZO-0.25, SLBTZO-0.50.

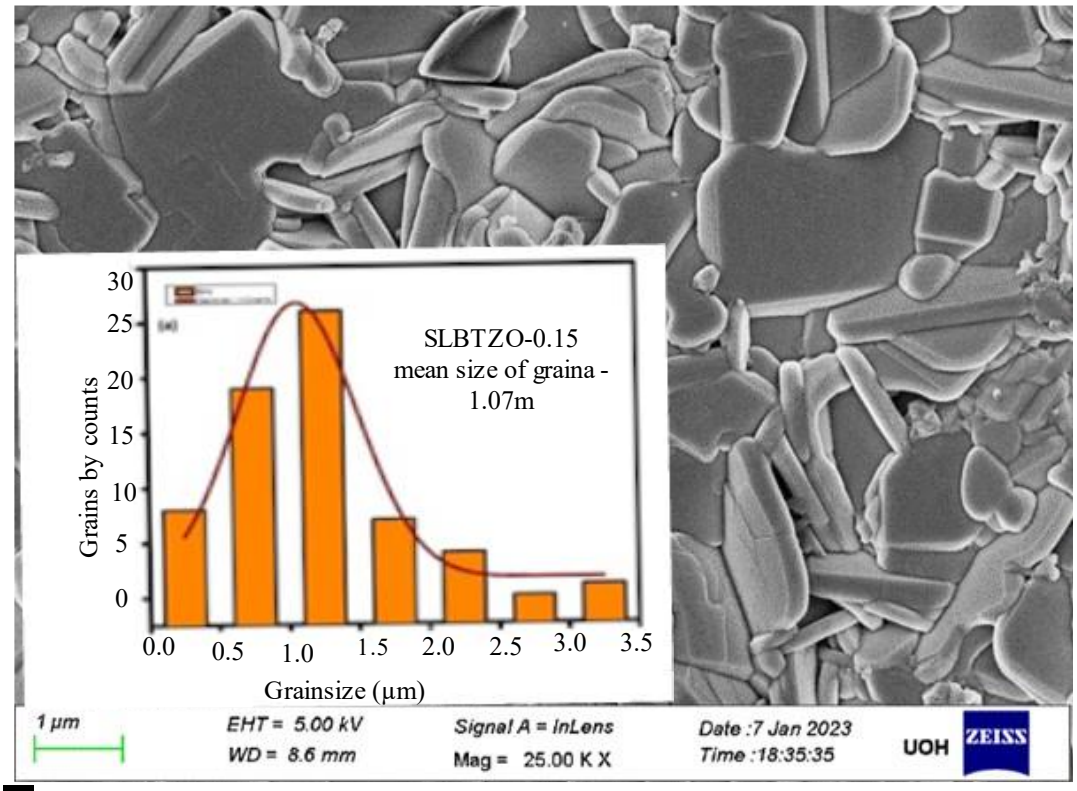

(a)

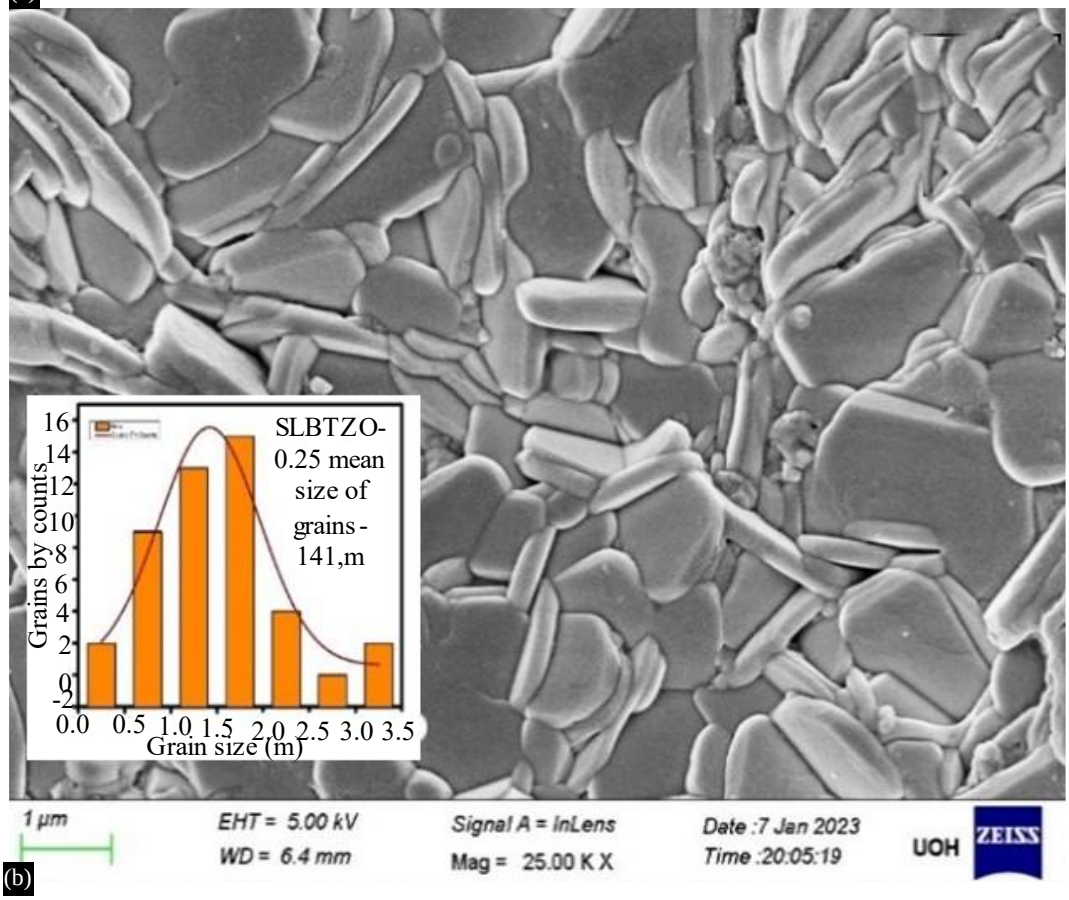

(b)

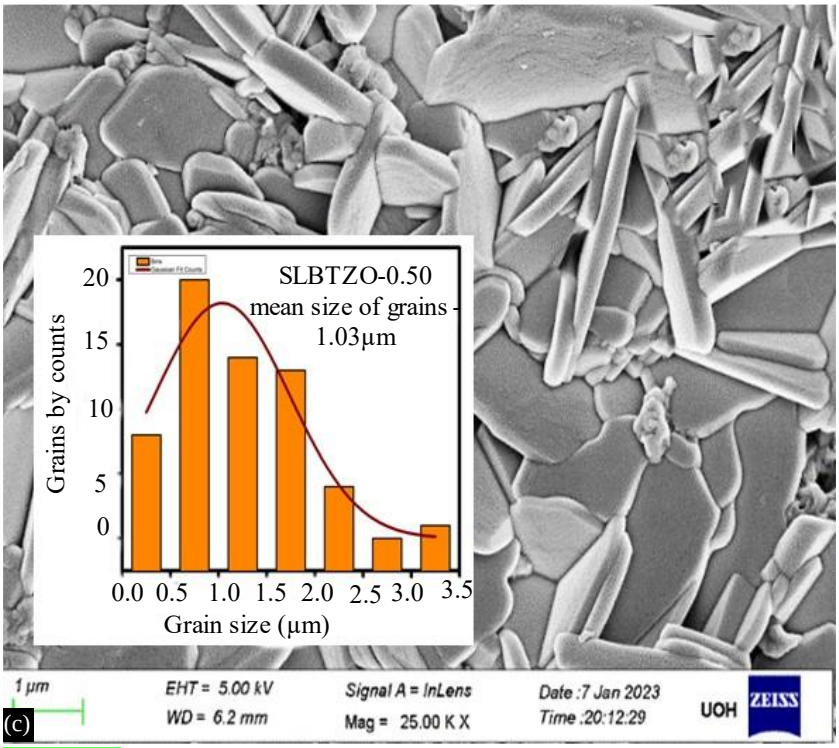

Figure 2. (a-c) The SEM images and grain size distribution of SLBTZO-0.15, SLBTZO-0.25 and SLBTZO-0.50 samples.

Raman Spectroscopy

Raman spectroscopy is generally used to understand the local ordering of modified systems in a subtle way. The results are helpful to correlate the X-ray data. A Raman spectrum of the SLBTZ-0.15, SLBTZO-0.25, SLBTZO-0.50 is shown in the Figure 3(a-c), in the range of 0 to 1200 cm^{-1}. In order to pinpoint the exact mode, the data was fitted in to Gaussian curves. The Raman modes were mentioned in the Figure 3(a-c), based on the fitted graph. The thin solid lines shown in the fitted graph are the individual modes and the thick solid line with open circle indicates total fit to the experimental data. . The presence of Ti-O, Zr-O, Bi-O, La-O and Sr-O bonds certainly reflect as vibrational modes in Raman spectra. The Raman mode observed above 150 $cm^{-1}$is being considered as the characteristic feature of layer-perovskite. Ti-O/Zr-O bonds locate beyond the 200 cm^{-1} (270, 560 and 780 cm^{-1}). The Raman vibrational mode observed at nearly 270 cm^{-1} indicates the torsional bending of TiO_6 octahedral. This is considered as B_{1g} mode. The modes observed at 560 and 754 cm^{-1} explains TiO_6 stretching mode vibrations. These modes correspond to B_{2g} and B_{3g} explain A-O bond. The present results were found to be consistent with the reported values [11, 12]. Broad Raman peaks observed 560 and 880 cm^{-1} is attributed to the Zr^{+2} replacements in Ti-site. No changes is seen in c-parameters (see Table.1) and variation observed in a and b-parameters confirms ab-plane vibrations. On account of the Ti atoms were easily affected strongly. A slight shift in the vibrational mode corresponds to the ab-plane of oxygen atom or TiO_6 octahedral.

Impedance and Modulus Analysis

Figure 4(a-c) shows the variation of imaginary part of impedance Z″ and M″ plots at different temperatures (up to 500^0c) for different La- concentrations in a semi-logarithmic scale. The magnitude of Z″ deceases with increasing frequency and the Z″ peak maximum are found to shift towards higher frequency side. This suggests that the presence of two relaxations. A decrease in the magnitude of Z″ with temperature indicates negative temperature coefficient of resistance (NTCR). Moreover, the decease of dispersion with increase of La-modification suggests the increase of space charge due to accumulation at grain boundaries [13–15].

It is also seen that the Z″ spectroscopic curves are not symmetric about the frequency and the broadness also increases with the temperature. The asymmetric and temperature dependent peaks indicate non-Debye type or deviation from ideal Debye curve. Moreover, the dielectric relaxations are attributed to the thermally activated charge carriers and can be generally understood by modulus spectroscopy data. It is a known fact that the impedance and modulus spectra give information about largest resistance and smallest capacitance of the compounds. The complex data can be extracted from the impedance data with the help of equation given.

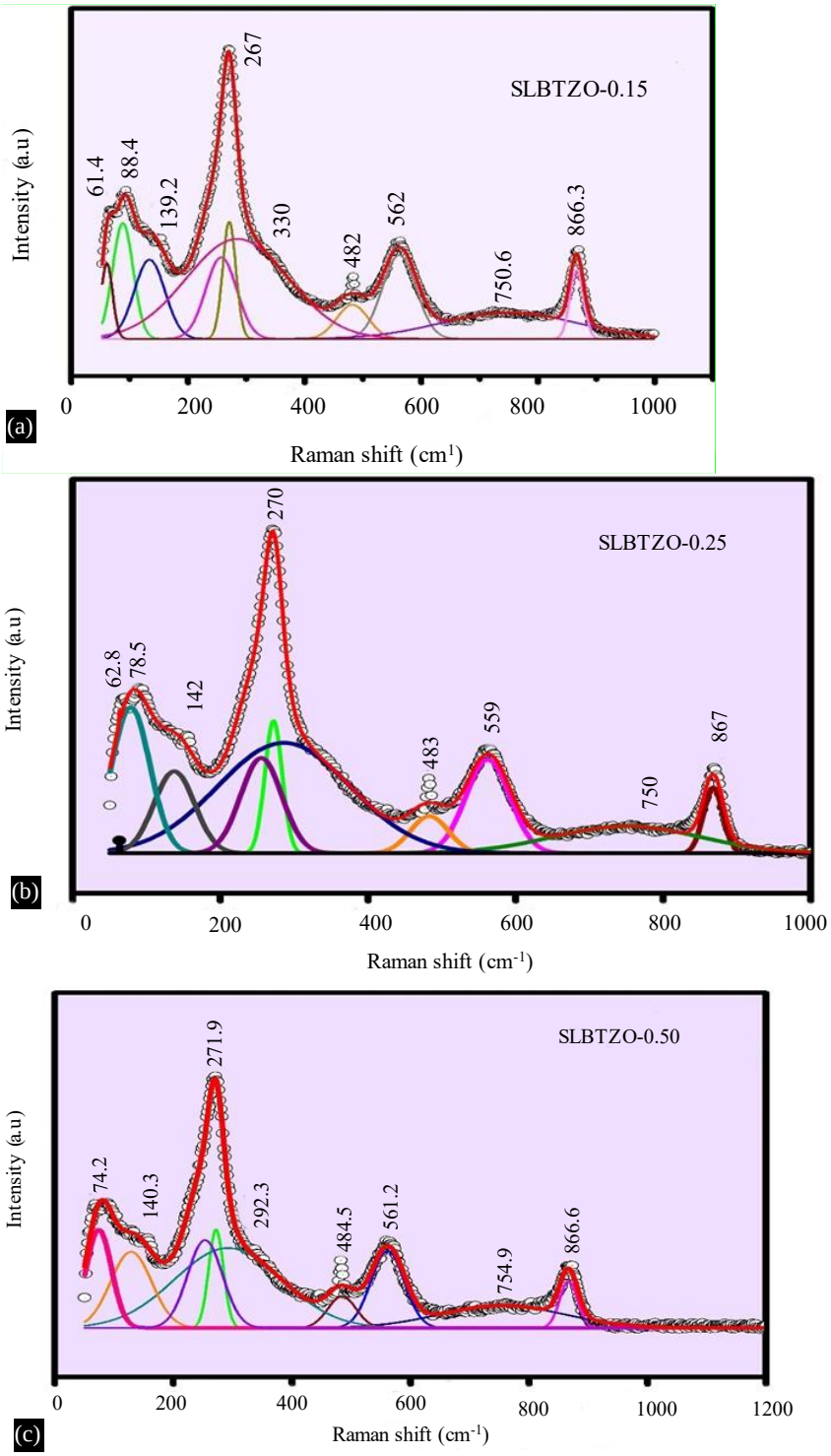

Figure 3. (a-c) Raman spectra of SLBTZO-0.15, SLBTZO-0.25, SLBTZO-0.50.

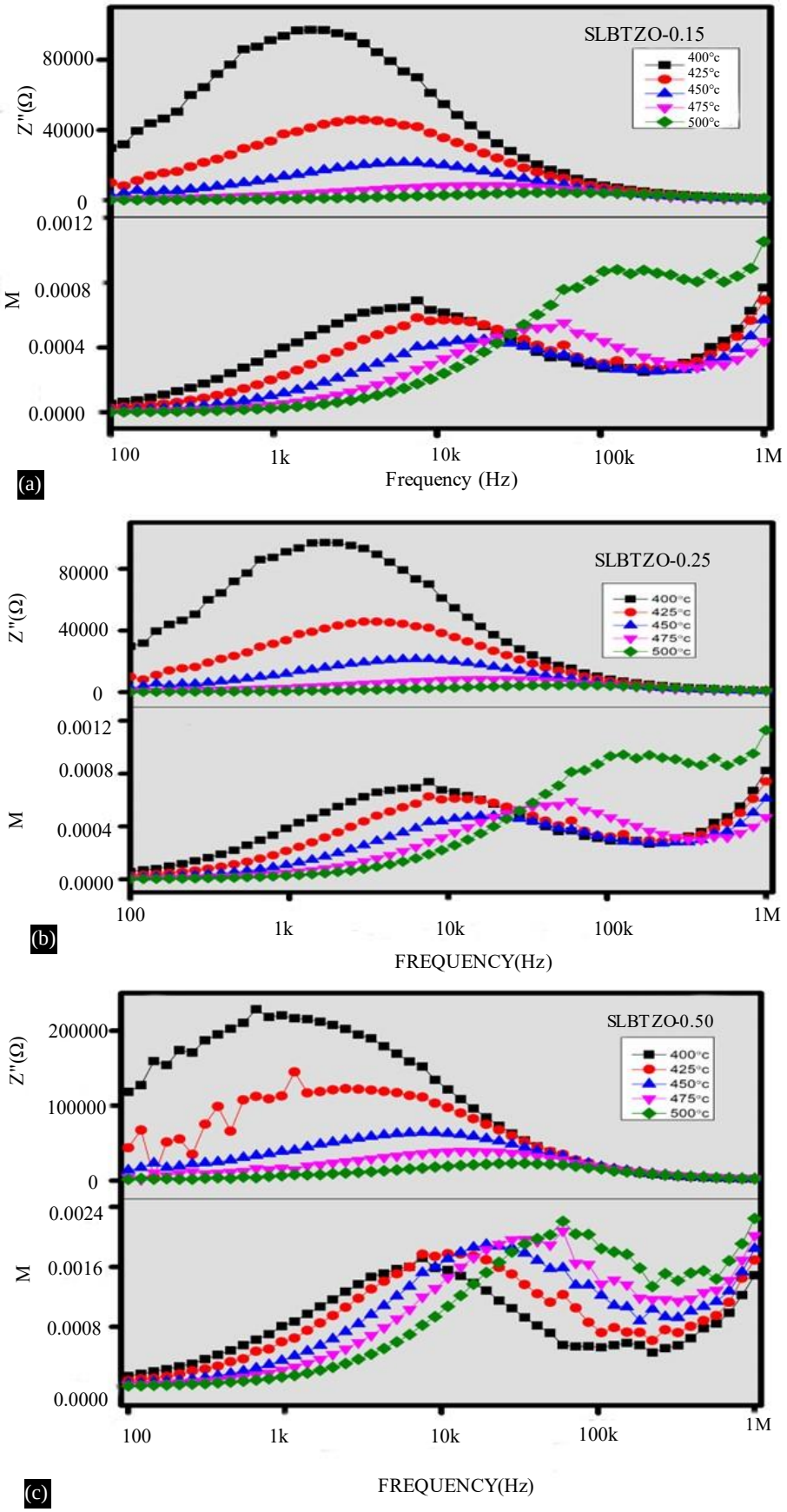

Figure 4. (a-c) Z″ and M″ plots of SLBTZO-0.15, SLBTZO-0.25, and SLBTZO-0.50.

M″ decreases and the peak shift towards higher frequency with the increase of temperature and again raise near 500^0 C. This clearly indicates a changeover mechanism of short-range order to long- range order. A shift M″ peak towards higher frequency side with increase in temperature suggests that the relaxation process is due to thermally activated process, as suggested earlier. An increase in M″ at higher frequency region and appear to merge into the single value. This indicates that the presence of accumulation of defects at grain interfaces. The asymmetric M″ curve also suggest a deviation from Debye nature. Nearly at zero value of Z″ in low frequency region, suggest the electrode polarization. With the increase of La-concentration in the chemical composition, an increase of Z″ of sample SLBTZO-0.50 is attributed to the DPT nature of the sample.

Figure 5(a-c) shows cole-cole plots for SBLTZO-0.15, SBLTZO-0.25, SBLTZO-0.50. The two semi circulars shown in the plot explain grain and grain boundary contributions of the samples. In the present study the semicircles were found be depressed nature like Debye, where the centers of semicircles lie on Z′ axis. Based on the RC-equivalent circuit, the resistance, capacitance of both grain and grain boundary were calculated and listed in Table 2.0. From the Table, the grain, grain boundary resistance and capacitance values were found to decrease with increasing temperature. From this, one can say that the conductivity increases with increasing temperature for all the samples. This is clearly an indication of NTCR behaviour of the sample. Grain and grain boundary resistance increases with increasing the La-concentration. Based on the high grain resistance values, one can predict that the grain boundary or its interface resistances are the dominantly in the overall conductivity of the material. This clearly indicates that the presence of charge carriers inside the grain interfaces and extrinsic charge carriers play a role in the conduction mechanism.

Table 2. Grain resistance and grain boundary resistance of all samples.

Compound	$R_g(\Omega)$	C_g (F)	$R_{gb}(\Omega)$	C_{gb} (F)
SBLTZO-0.15	7680	1.608×10^{-9}	4740	8.64×10^{-5}
SBLTZO-0.25	8550	1.26×10^{-9}	5800	1.1×10^{-5}
SBLTZO-0.50	38600	5.8×10^{-10}	24600	6.98×10^{-6}

Conduction Mechanism

In order to understand the transport behaviour of La modified SBT temperature dependence of AC-conductivity shown in Figure 6(a-c).

AC- conductivity was determined using the following formula.

$$\sigma' = (Y' * t/a) \quad (5)$$

Here Y represents the real part of admittance, t represents that thickness of the samples and A represents the cross-section area of the samples. The variation of AC- conductivity with the frequency can be divided into two distinct regions namely lower and higher frequency regions respectively. The ac-conductivity in the two regions can be explained as:

i. Frequency independent behavior of ac- conductivity at the lower frequency region, marked as region-I. This is attributed to the long-range movement of mobile charge carriers.
ii. In the high frequency region (region II), the conductivity is found to increase with frequency. This is generally attributed to the hopping of charge carriers within the cluster or region.
iii. A crossover is observed in region-II, known as hopping frequency is found to shift towards high frequency side with increasing temperature.
iv. An order of jump in the conductivity, at high frequency, also indicates the increase of mobile charge carriers. This crossover region also indicates the enhancement charge carriers through the grain boundary region. The same is consistent with the complex impedance (Cole-Cole) plots.

An increase of conductivity with increasing frequency and temperature is being attributed to the hopping electrons between $Ti^{3+} \leftrightarrow Ti^{4+}$ and defects such as oxygen vacancies. The excess electrons and oxygen vacancies are formed in the following reduction reaction.

$$O_o^* \rightarrow \frac{1}{2} O_2 + \ddot{V}_o + 2\bar{e} \quad (6)$$

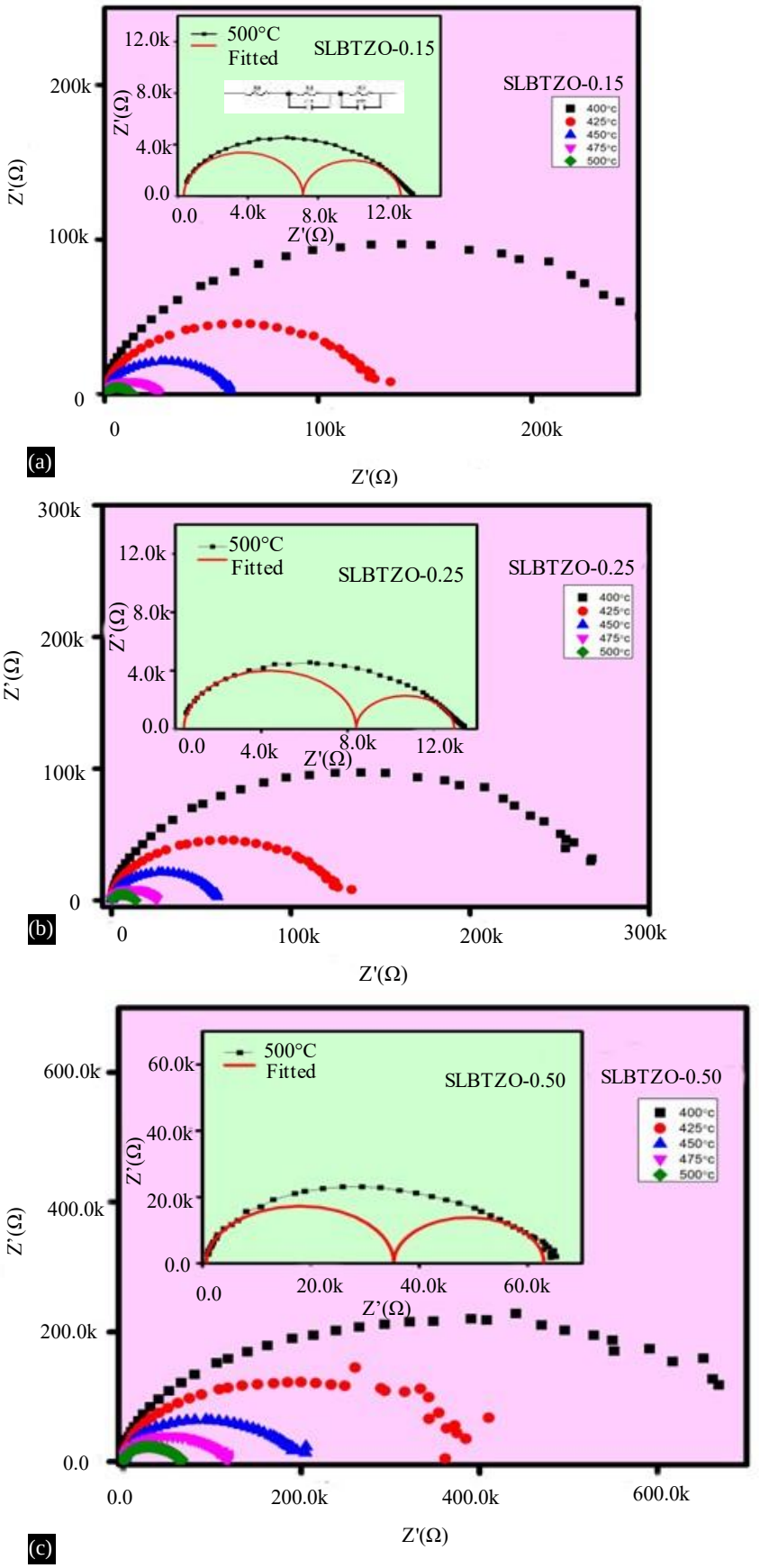

Figure 5. (a-c) Cole-Cole plots of SLBTZO-0.15, SLBTZO-0.25, and SLBTZO-0.50 samples.

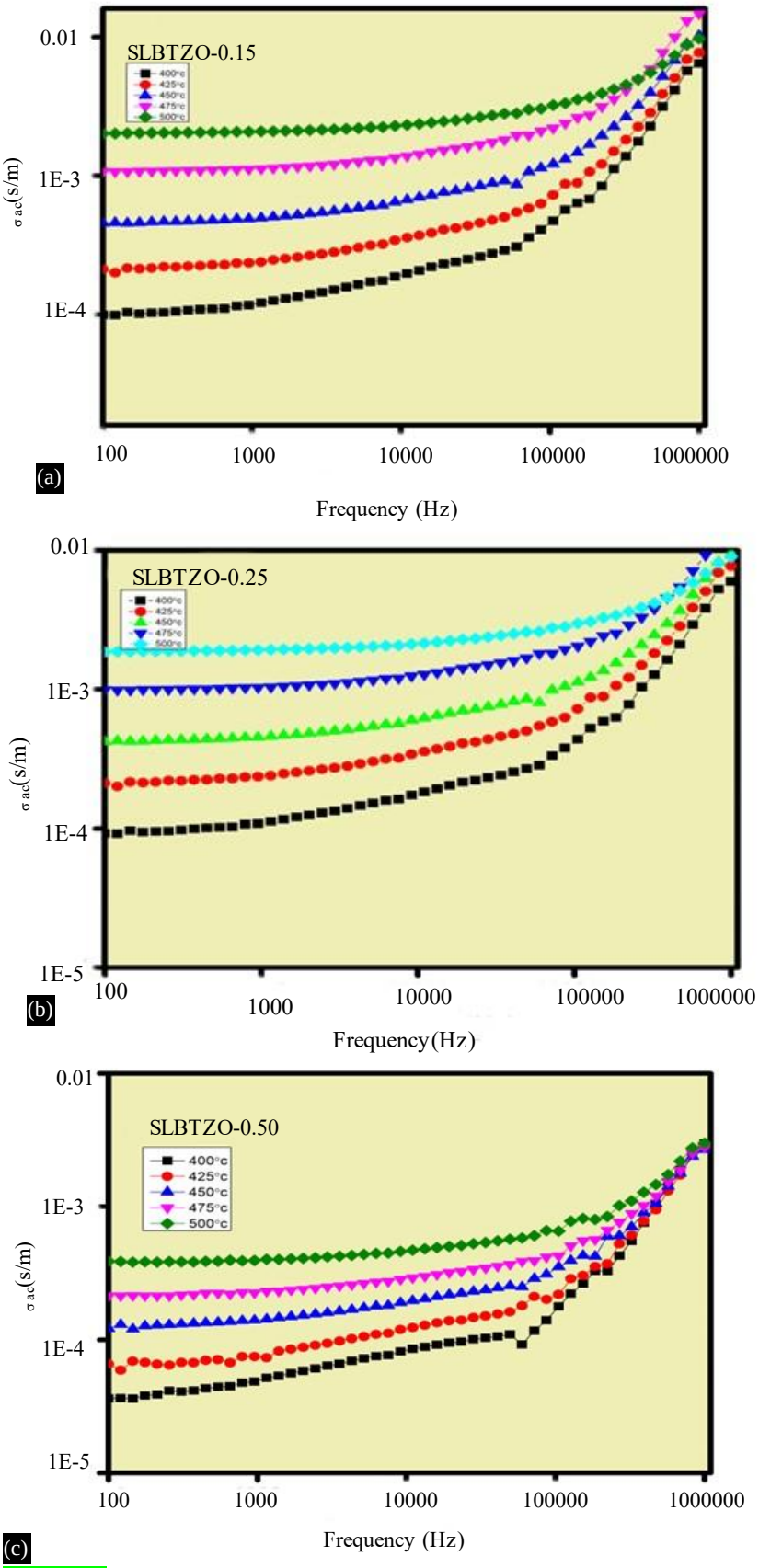

Figure 6. (a-c) The variation of ac conductivity with frequency at different temperatures for SLBTZO-0.15, SLBTZO-0.25 and SLBTZO-0.50 samples.

Where O_o^* is the neutral oxygen state and $\ddot{V}_o$ is doubly ionized Vacancy. This doubly ionized vacancy cannot trap any electron as it is a two-fold positive entity. This entity is thermally activated and hence enhances the conduction process at higher temperature in perovskite materials. In addition, due to ionic environment at A-site (chemical inhomogeneity on account of Sr^{+2} and Bi^{+3}) the vacancies (oxygen) play the vital role in layered compounds. Since Zr-O bond strength is weaker than the Ti-O bond, the distortion (TiO_6) becomes weaker and hence it leads to reduction of both dielectric constant as well as transition temperature. The result is consistent with grain size, as deceasing of the grain size causes reduction in the transition temperature. Moreover, the larger grains in the domain walls are free, and the movement is not restricted. Therefore, at the grain interface region, it contributes an additional pinning behaviour to the domain walls. The presence of O_2 vacancies act as space charge and contributes electrical polarization this in turn leads to the broad ferroelectric peak in ε' verses temperature curve. This is one of the most important features of the perovskite structure with different phase transition. The diffusion nature is mainly due to the compositional fluctuation and structured disorder nature as mentioned earlier.

Dielectric Study

The dielectric constant verses temperature, drawn at different frequencies, is shown in the Figure 7 (a-c). It is observed that dielectric constant decreases with increases in La content. This is attributed to the increase in lattice parameter-a and associated relaxation of the structural distortion [16–20]. It is also observed that with increasing La-content the transition temperature (T_m) shifts towards lower temperature side The reduction in dielectric transition temperature is due to the incorporation of larger ionic radii La^{+3} ion in Bi^{+3}ion. This intern enlarges the unit cell and lattice distortion. The decrease of orthorhombic distortion (shown in Table 2) explains the stability of the perovskite blocks [20-23]. Inset Figure7(a-c) shows dielectric the loss verses temperature graph obtained at different frequencies. It is observed that with the increasing of the La-concentration the dielectric loss decreased.

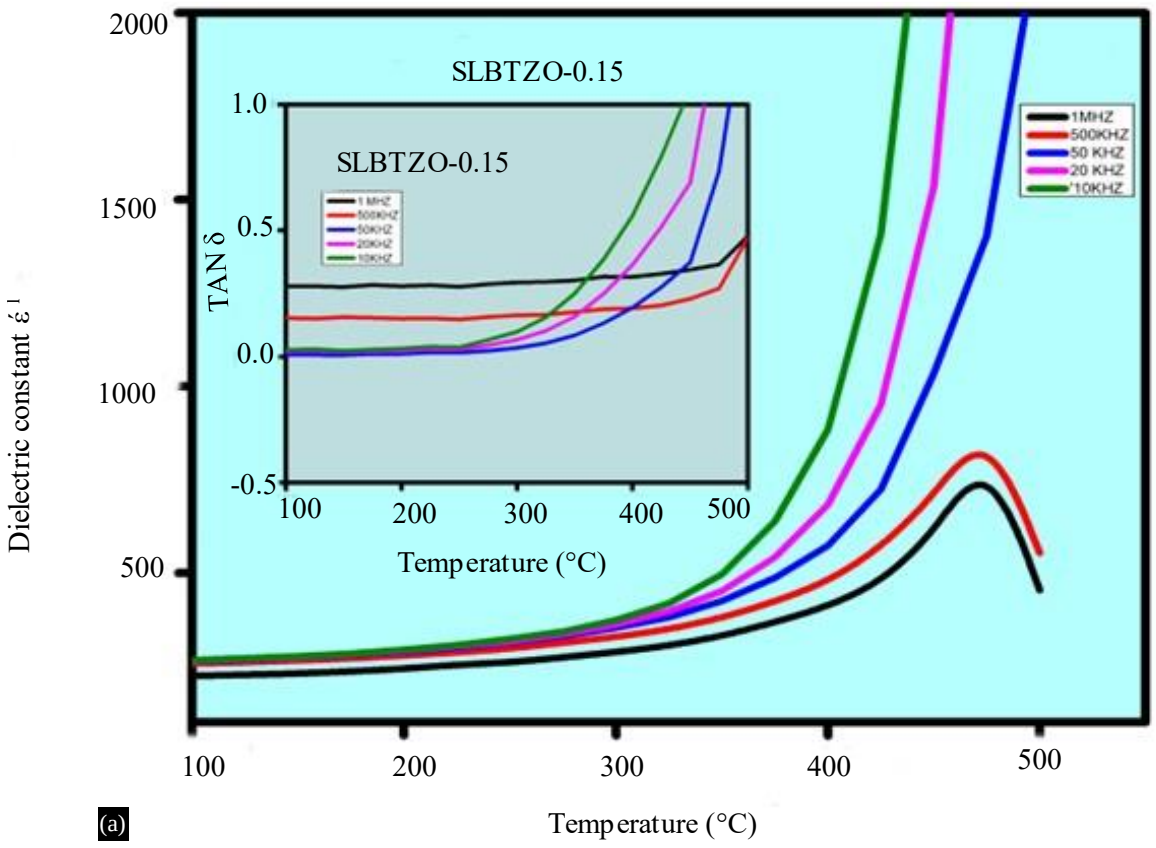

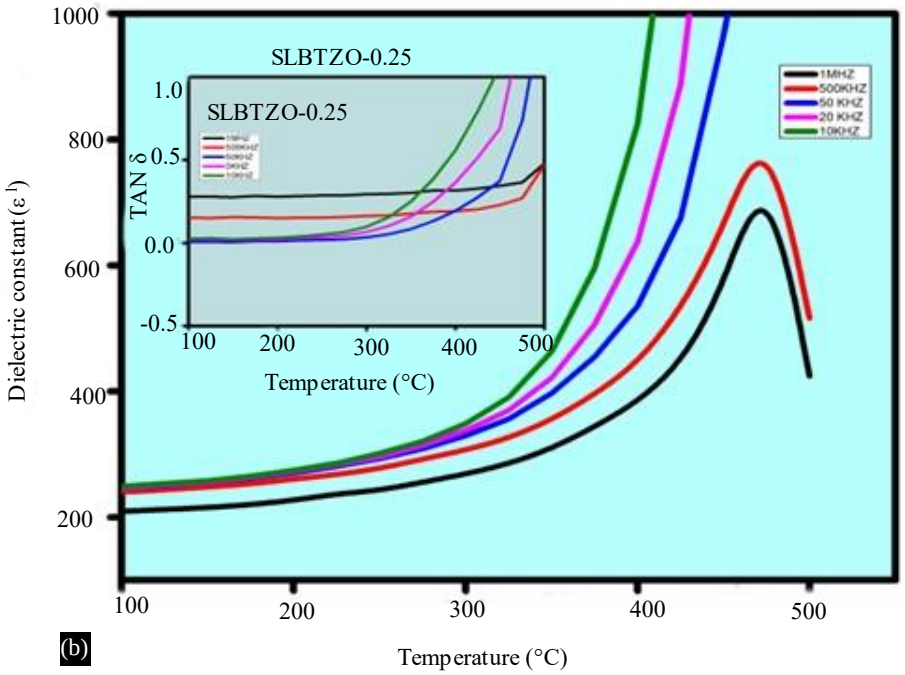

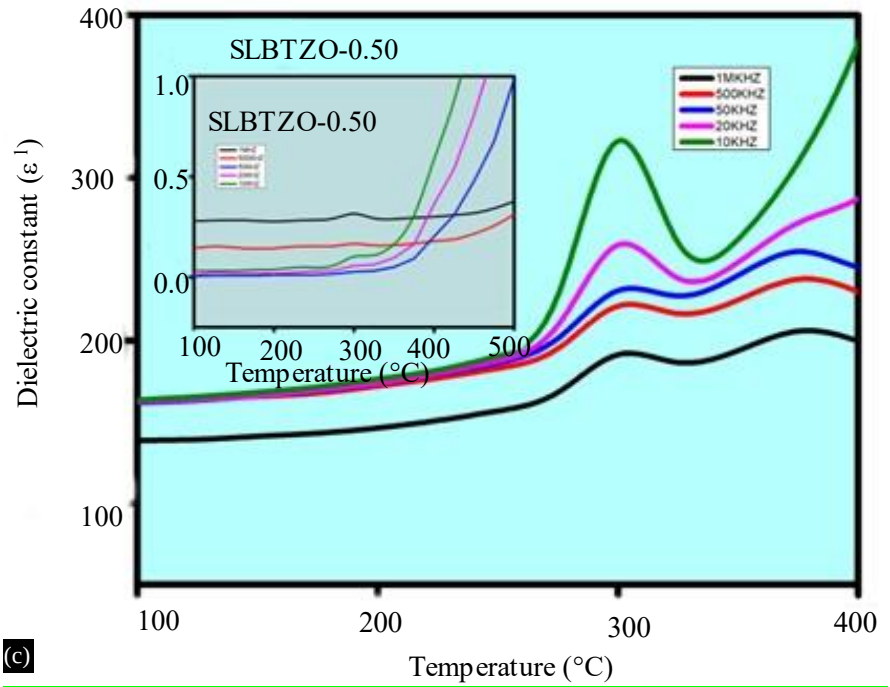

Figure 7. (a-c) The variation of dielectric constant with temperature at different frequencies for SLBTZO-0.15, SLBTZO-0.25 and SLBTZO-0.50samples.

CONCLUSIONS

La modified SBTZ materials were prepared by conventional solid-state route. The structural, Raman, impedance and dielectric properties were carried out on $SrLa_xBi_{4-x}Ti_{3.85}Zr_{0.15}O_{15}$ (x= 0.15,0.20,0.50) ceramics. XRD patterns revealed that all the ceramics are of single phase. The lattice parameters were found to decrease with the increasing of the La- concentration. Raman modes explain the preferred substitution of La^{+3} at the A-site of the pseudo-perovskite blocks. A shift in maximum XRD intensity peaks also confirms the same. The transition temperature is found to decease with increasing the La-content in the title compound. Moreover, the diffusion nature also found to increase with the La-concentration. In addition, the conductivity is attributed to the small and large polarization mechanism.

An increase in the grain resistance with La- modification causes the development of internal stress within the region and changes the transition temperature. The combined impedance and modulus spectroscopic plots show temperature dependent relaxation of non-Debye type. Spectroscopic relaxation peaks were found to shift towards higher frequency side. Ac- conductivity data shows that the charge carriers of long -range mobility. The low dielectric loss suggests the presence of oxygen vacancies which are responsible for long range migration of charge carriers.

Acknowledgements

The research work is partially funded by the grants of OU-DST -PURSE program, India.

REFERENCES

1. Reaney I.M, Damjanovic D, Crystal structure and domain-wall contributions to the piezoelectric properties of strontium bismuth titanate ceramics, J. Appl. Phys.1996;80: 4223–4225. https://doi.org/10.1063/1.363301.
2. Park B.H, Kang B.S, Bu S.D, Noh T.W, Lee J, Jo W, Lanthanum-substituted bismuth titanate for use in non-volatile memories, Nature. 1999; 401: 682–684. https://doi.org/10.1038/44352.
3. Yao Y.Y, Song, C.H., Bao P., Su D, Lu X.M, Zhu J.S, Wang Y.N, Doping effect on the dielectric property in bismuth titanate, J. Appl. Phys. 2004;95: 3126–3130. https://doi.org/10.1063/1.1649456.
4. Khokhar. A, Goyal P.K, Thakur O.P, Shukla A.K, Sreenivas K, Influence of lanthanum distribution on dielectric and ferroelectric properties of Ba Bi $_{4-x}$ La $_{x}$ Ti $_{4}$ O $_{15}$ ceramics, J. Mat Chem Phys., 2015;152: 13–25. https://doi.org/10.1016/j.matchemphys.2014.11.074.
5. Zhu.J, Chen.X, Shen.J, Lanthanum distribution in Sr $Bi_{4-x}La_xTi_4O_{15}$, J. Mat. Lett., 2005;59: 1581–1584. https://doi.org/10.1016/j.matlet.2005.01.027.
6. Chen.J, Yun.Q, Gao.W, Bai. Y, Nie. C, Zhao. S, Improved ferroelectric and fatigue properties in Zr doped Bi_4 Ti_3 O_{12} thin films, J. Mat. Lett., 2014;136 :11–14. https://doi.org/10.1016/j.matlet.2014.07.182.
7. Chakrabarti. A, Bera. J, Structure and relaxor behavior of $BaBi_4Ti_{4-x}Zr_xO_{15}$ ceramics, Current App. Phys., 2010;10:574–579. https://doi.org/10.1016/j.cap.2009.07.027.
8. Nayak. P, Badapanda. T, Singh A.K, S. Panigrahi, An approach for correlating the structural and electrical properties of Zr $^{4+}$ -modified SrBi $_{4}$ Ti $_{4}$ O $_{15}$ /SBT ceramic, RSC Adv.2017;7 :16319–16331. https://doi.org/10.1039/C7RA00366H.
9. Rout S.K, Sinha. E, Hussian. A, Lee. J.S, Ahn C.W, Kim I.W, Woo S.I, Phase transition in $ABi_4Ti_4O_{15}$ (A=Ca,Sr,Ba) Aurivillius oxides prepared through a soft chemical route, J Appl Phys. 2009;105: 024105(1-6). https://doi.org/10.1063/1.3068344.
10. G, Sreekanth. T, Tripathy. N, Sarah. P, Structural and dielectric investigation of rare earth modified $SrBi_4Ti_4O_{15}$ ceramics synthesized by high energy ball milling method, Mater Today Proc.2023;92 :667–670. https://doi.org/10.1016/j.matpr.2023.04.151.
11. Nayak. P, Badapanda. T, Panigrahi. S, Dielectric, ferroelectric and conduction behavior of tungsten modified $SrBi_4Ti_4O_{15}$ ceramic, J Mater Sci: Mater Electron.2016;27 :1217–1226. https://doi.org/10.1007/s10854-015-3878-2.
12. Hao. H, Liu H.X, Cao M.H, Min X.M, Ouyang S.X, Study of A-site doping of $SrBi_4Ti_4O_{15}$ Bi-layered compounds using micro-Raman spectroscopy, Appl. Phys. A.2006;85: 69–73. https://doi.org/10.1007/s00339-006-3651-8.
13. Bhargavi G.N, Khare A, Badapanda T, Anwar M.S, Brahme N, Electrical characterizations of $BaZr_{0.05}Ti_{0.95}$ O_3 perovskite ceramic by impedance spectroscopy, electric modulus and conductivity, J Mater Sci: Mater Electron.2017;28:16956–16964. https://doi.org/10.1007/s10854-017-7617-8.
14. Ahmad. Z, Mishra. A, Abdulrahim S.M, Touati F, Electrical equivalent circuit (EEC) based impedance spectroscopy analysis of HTM free perovskite solar cells, J Electroana. Chem., 2020;871: 114294. https://doi.org/10.1016/J.JELECHEM.2020.114294.
15. Sharma V.K, Nathawat R, Rathore S.S, Dielectric properties correlation with microstructure in ABi $_{4}$ Ti $_{4}$ O $_{15}$ (A = Sr, Ba) bismuth layered ferroelectrics, Mater Adv.2022; 3:4890–4898. https://doi.org/10.1039/D2MA00333C.

16. Raymond O, Font R, Suárez-Almodovar N, Portelles J, Siqueiros J.M., Frequency-temperature response of ferroelectromagnetic Pb (Fe1⁄2Nb1⁄2) O3 ceramics obtained by different precursors. Part I. Structural and thermo-electrical characterization, J Appl Phys.2005;97: 084107(1-8). https://doi.org/10.1063/1.1870099.
17. Long C, Fan H, Li M, Ren P, Cai Y, A candidate for lead-free ultrahigh-temperature piezoelectrics: the excellent electro-mechanical properties of Aurivillius oxides, $Ca1-5_xLi_{2x}Nd_{2x}\square xBi_2Nb_{2-2x}Sc_xW_xO_9-1.5_x$, Cryst Eng Comm.2013;15: 10212-10221. https://doi.org/10.1039/c3ce41594e.
18. Sindhu M, Ahlawat N, Sanghi S, Agarwal A, Dahiya R, Ahlawat N, Rietveld refinement and impedance spectroscopy of calcium titanate, Curr. App. Phys., 2012;12:1429–1435. https://doi.org/10.1016/j.cap.2012.03.034.
19. Tadashi Takenaka K.S, Electrical Properties of Grain-oriented Ferroelectric Ceramics in Some Lanthanum Modified Layer-structure Oxides, [J]. Ferroelectrics.1981;1: 769–772.
20. Seth V.K, Schulze W.A, Grain-oriented fabrication of bismuth titanate ceramics and its electrical properties, IEEE Trans Ultrason Ferroelectr Freq Control.1989;36 :41–49. https://doi.org/10.1109/58.16967.

